Lab on a Chip

PAPER

View Article Online
View Journal



Cite this: DOI: 10.1039/c9lc00254e

# Microfluidic blood vasculature replicas using backside lithography†

Marianne Fenech, [ac] Vincent Girod, [b] Viviana Claveria, [c] Sebastien Meance, [b] Manouk Abkarian[c] and Benoit Charlot *[b]

Received 14th March 2019,
Accepted 29th April 2019

DOI: 10.1039/c9lc00254e

rsc.li/loc

Blood vessels in living tissues are an organized and hierarchical network of arteries, arterioles, capillaries, veinules and veins. Their sizes, lengths, shapes and connectivity are set up for an optimum perfusion of the tissues in which they deploy. In order to study the hemodynamics and hemophysics of blood flows and also to investigate artificial vasculature for organs on a chip, it is essential to reproduce most of these geometric features. Common microfluidic techniques produce channels with a uniform height and a rectangular cross section that do not capture the size hierarchy observed *in vivo*. This paper presents a new single-mask photolithography process using an optical diffuser to produce a backside exposure leading to microchannels with both a rounded cross section and a direct proportionality between local height and local width, allowing a one-step design of intrinsically hierarchical networks.

## Introduction

Blood is a non-Newtonian complex fluid consisting of a dense suspension of cells in plasma. This set of cells is composed mainly of red blood cells (RBCs) but also in a much smaller number, white blood cells and platelets. Due to its particulate nature, blood flow in vascular networks is complex and several remarkable properties are associated with it. First, blood is a shear-thinning fluid as quantified by Chien *et al.*[1] in the late sixties. Blood viscosity drops when the shear rate increases. Two different regimes of shear rates govern shear thinning: when blood flows in large vessels, therefore at low shear rate, viscosity decrease is governed by the mechanisms of disassembly of large aggregates formed by RBCs due to depletion forces present in the plasma. On the other hand, when blood flows into smaller vessels and therefore at high shear rate, the deformability of the cells themselves becomes the major determinant of shear thinning.[2]

In addition, the Fåhræus–Lindqvist effect links the viscosity of the blood with the vessel diameter. This effect is due to the appearance of a cell layer in the vicinity of the walls where the shear rate is maximal and tends to concentrate cells in the center of the vessels. Thus, it lowers blood apparent viscosity when it flows into vessels down to 10 μm diameter.

One of the keys to understanding hemophysics[3] and blood flow dynamics is to build replicas of vascular networks with a geometry as close as possible to that in natural networks in order to observe the movements of RBCs under a microscope using high-power illumination and a high-speed camera. Microfluidics and in particular microfluidic circuits made of PDMS have the ability to reproduce vascular networks that represent a model of blood microcirculation.[4–6] The transparency of PDMS as well as the micrometric size of patterns makes it possible to obtain replicas of vascularization that can be observed under a microscope. PDMS replicas of vascular networks are an important tool for studying the distribution of RBC velocities,[7–9] cell deformations under high shear stresses,[2] oscillations of capillary blood flows,[10] or the dynamics of RBC aggregation.[11] Recent advances are now integrating interactions between circulating cells and a model endothelium[12–14] or polymer construct that mimics the glycocalyx.[15] In addition to hemophysics studies, replicas of vascular networks can be used to monitor the quality of stored blood,[16] as a diagnostic device for pathologies that affect blood rheology, to study the effect of cell deformability on the behavior of a blood circulation network[17] and finally to simulate vascular anomalies.[18] These microfluidic circuits are two-dimensional projections of a network that is tridimensional by nature. Although such a projection in a plane cannot accurately represent the connectivity of a 3D network, this represents an approximation that may be acceptable if care is taken to maintain the section and length distributions of the vessels as well as the branching and loop statistics of a

[a] Department of Mechanical Engineering, University of Ottawa, Ottawa, Canada
[b] Institut d'Electronique et des Systèmes IES, CNRS, University of Montpellier, Montpellier, France. E-mail: benoit.charlot@umontpellier.fr
[c] Centre de Biochimie Structurale CBS, CNRS, INSERM, University of Montpellier, France

† Electronic supplementary information (ESI) available. See DOI: 10.1039/c9lc00254e

natural vascular network. This is clearly a disadvantage in terms of biomimetism but an advantage for microscopy.

Vascular networks have complex geometries made of interconnections, bifurcations and loops with vessels whose diameter varies dramatically (typically 4 mm down to 5 μm). The main function of this hierarchical network is to perfuse the tissues. The capillary network, also called capillary bed, is deployed in three dimensions in organs and tissues for optimal irrigation. Then, the venous network, out of the capillary bed harvests the cells that made the exchanges to bring them back to the heart. Recent progress in imagery now allows reconstruction of the exact topology of the vasculature of a whole organ,[19] including the capillary bed with thin capillaries.

After a short introduction to techniques developed for producing artificial vasculature, we report here an original technique that allows producing a microcirculation replica that mimics the geometry of natural vascular networks. The microfabrication process presented here involves only one photomask and uses the diffusion of UV light from the bottom of a negative photoresist layer to achieve a gradation of thickness from a single exposure. Microfluidic vascular networks produced with this technique are then used to observe particularities of blood flows.

## Vasculature network replicas

Vascular networks have a specific geometry that depends on the organ where they deploy. However, we can observe common features such as tubular vessels, a distribution of vessel diameters between arteries, arterioles, capillaries, veinules and veins as well as the presence of loops. Several techniques have been developed so far to reproduce artificial networks with the specifications of transparency, surface roughness, minimum size of around 5 μm, circular cross section and ease of fabrication.

### Conventional photolithography

Replica moulding technologies using SU-8 photoresist on silicon and PDMS casting are the main techniques that have been employed for the fabrication of artificial networks. Although these techniques satisfy the specifications of transparency and micrometric precision, they do not faithfully reproduce the geometry of a vascular network. The main limitation concerns, in the first place, the fact that microfluidic circuits manufactured from a counter mould of a SU-8 photoresist, are composed of channels with rectangular sections but, above all, having all the same height. Conversely, a natural vascular network consists of vessels of more or less circular sections of different diameters showing a very wide range of diameter (5 μm to 4 mm). When using standard photolithography techniques to reproduce a vascularization pattern, one can obtain a geometry similar to that shown in Fig. 1(bottom right) with uniform thickness and straight walls, which is far from the geometry shown in Fig. 1(bottom left).

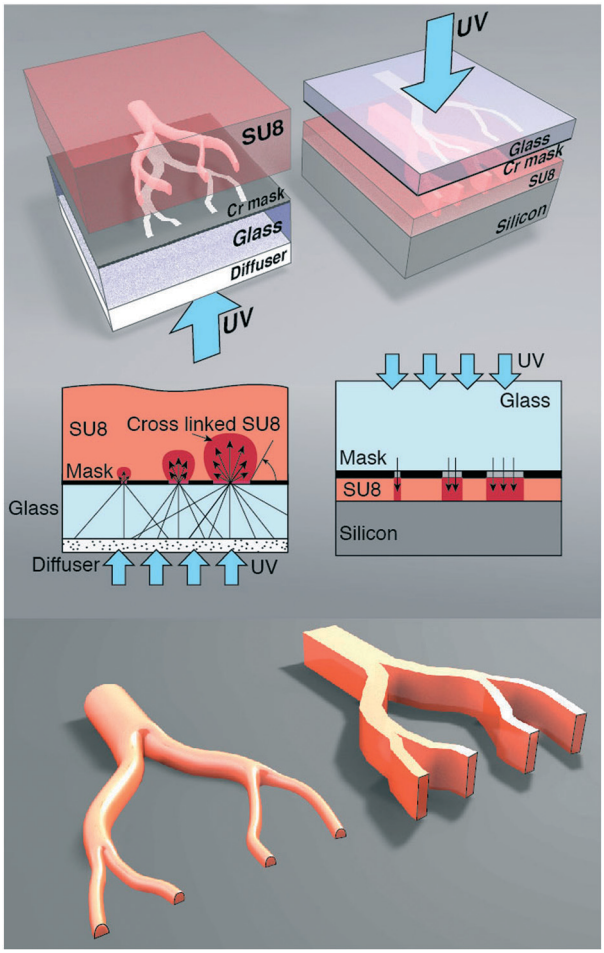


**Fig. 1** Principle of the microfabrication processes for artificial vascular networks. On the left side the principle of the proposed technique compared with, on the right side, standard topside photolithography as well as 3D schematic of the geometries of vascular networks obtained with these techniques.

Several research teams have then tried reproducing the complex geometry of vascular networks and in particular the specification of circular cross sections. One of the first solution presented by Cokelet *et al.* in 1993 (ref. 20) is to use wet etching of glass substrates with hydrofluoric acid, allowing one to obtain circular section channels. Another solution is, for example, to first produce a microfluidic circuit of rectangular cross sections and then to introduce a non-crosslinked PDMS mixture to completely fulfill the channels. Finally, the injection of air under pressure creates a meniscus effect smoothing the channel cross sections.[21,22] Although these techniques indeed make it possible to round the angles, they are complex to implement. Furthermore, they do not make it possible to obtain a gradation of the heights of the channels as a function of their widths. The laser ablation technique has also been investigated to directly write networks onto a polymer. If this technique allows indeed the production of multiple-level microfluidic channels[23] it is at the expense of a relatively high surface roughness.

A simple solution for obtaining channels with a circular section is to anneal a thermoplastic positive photoresists.[29,30] This makes it possible to round the profile of channels as a function of surface tension when the viscosity of the polymer decreases with temperature. Depending on the wetting angle of the polymer on the substrate, it is even possible to approach semicircular sections. However, when the channel widths exceed a certain threshold the profile begins to resemble the section of a red blood cell.

### 3D printing techniques

Additive fabrication and micro stereolithography technologies are currently under intense research efforts. These techniques have been employed successfully for the production of not only microfluidic devices but also microvasculature replicas.[24] One of the main advantages of these techniques is their ability to reproduce the actual 3D geometry of vascular networks. However, even though these techniques seem really promising they still do not have, for now, enough spatial resolution and sufficiently low surface roughness to be able to reproduce a capillary bed hierarchically connected to larger dendritic or reticulated networks. Finally, one technique that seems encouraging for the application described in this paper is the one developed by Lewis *et al.*[25] using fugitive inks or liquid metals.[26]

## Backside illumination photolithography

The solution we have chosen to explore in this work is backside lithography coupled to a light diffuser. This technique[31–33] consisted in exposing a photoresist through a lithography mask, not pressed and on the surface of a resin-coated sample, as in conventional photolithography techniques, but located on the surface of a transparent substrate, as sketched in Fig. 1. This solution therefore imposes an additional step, which is precisely the creation of the mask on the surface of the sample. This can be achieved either by deposition and engraving steps or by lift-off microstructuring on a glass substrate. Exposing a homogeneous resin thickness through the backside will lead to approximately the same resolution as that of a front-face lithography if the exposure doses are respected. The SU-8 negative photoresist, which is widely used in microfluidics, is very transparent in the 365 nm UV band. Therefore, a short exposure just below the necessary doses makes it possible to cross-link large thicknesses of SU-8 by eliminating at the same time the need of perfect contact between the lithography mask and the thick photoresist.

The use of a diffuser is the key element that allows height gradation as a function of width. The diffuser induces an effect that can be compared to micro-loading phenomena in plasma etching. An optical diffuser will thus diffuse the light from its surface according to its angular diffusion profile. The quality of the optical diffuser and in particular this angular diffusion profile is the critical parameter of this technique. Lee *et al.*[31] showed that the profiles obtained in negative photoresists, mainly SU-8, are directly linked to a function of the polar diffusion intensity curves. They showed in particular that it was possible to obtain angles of up to 45° between the photoresist and the substrate using an opal diffuser. Microfabrication results of an artificial vascular network produced with this technique are shown in Fig. 2. We can notice, in particular, the differences between this technique and the standard photolithography process (Fig. 2(e and f)).

## Materials and methods

### Network design

We designed an artificial network that is shown in Fig. 2 and 4. It contains one inlet, one outlet and an arbitrary tree of micro-channels of different widths that flare in tortuosities, bifurcations and loops. The geometry of this network was inspired from *in vivo* networks but not exactly representative of a natural vascular network[27] that followed Murray's law.[28] Nevertheless, it has been designed to show a distribution of channel sizes from 120 μm (inlet and outlet channels) down to 5 μm (capillaries) that respected the statistical distribution[27] of vessel sizes and lengths found in natural vascularization. The inlet, mimicking an arteriole, was consecutively divided into daughter branches of smaller width with the following succession of widths: 120, 75, 35, 22, 12 and finally 5 μm for the capillaries. The capillary bed, unlike the arteriole tree, is made up of several branches and loops. At the exit of the capillary bed, a network of veinules recovered the flows to concentrate them towards one unique outlet. This mask has been designed for the sole purpose of developing the technique presented here. The network spreads over a surface of 2.2 × 3 mm. The design has been made using Cadence Virtuoso (Cadence Design Systems, Inc. San Jose, CA, USA).

### Microfabrication

**Substrate.** The microfabrication process began with 5 × 5 cm and 500 μm thick glass slides (Paul Marienfeld GmbH, Lauda-Königshofen, Germany) that were previously cleaned with a piranha solution. Next, a 100 nm thick chromium layer was deposited on the whole surface by electron beam physical vapor deposition. A layer of AZ1518 photoresist (MicroChemicals, Ulm, Germany) is then spin-coated and prebaked at 110 °C for 1 min. The microcirculation pattern is transferred by contact photolithography, and the photoresist is developed in an alkaline solution. The mask is then defined by a wet etching process (chromium etching solution) resulting in a transparent network pattern. Finally, the remaining photoresist is stripped with acetone and oxygen plasma ashing. This chromium layer can be replaced by an aluminum one thick enough to be opaque to light with no consequence on the process.

**Adhesion layer.** A 1 μm thick layer of SU-8 2002 (MicroChem, Westborough, MA, USA) is then spin-coated on the

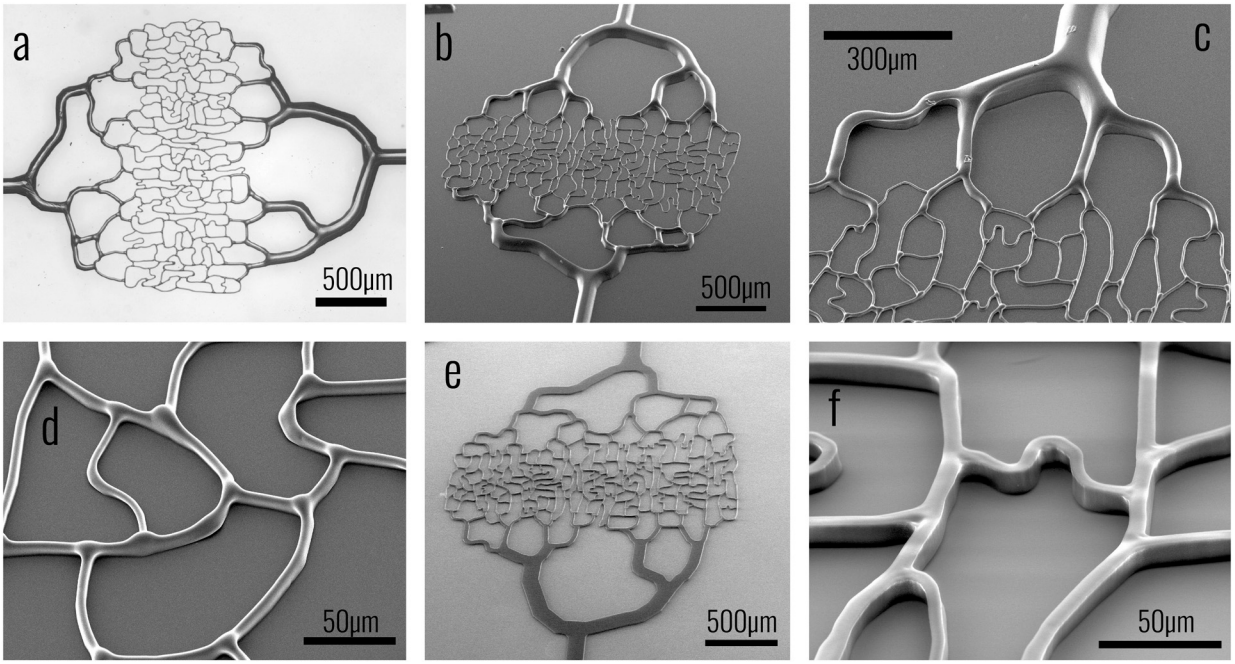


**Fig. 2** Images of artificial vascular networks. (a) Transmitted light optical photograph (bright field) of the PDMS replica. (b–d) SEM image of the SU8 mould made with the backside lithography technique at different magnifications. We can observe the gradation in height according to width of channels. (e and f) SEM image of the same network made with a conventional top side exposed SU8 on silicon technique. We can observe the uniform thickness (15 μm) and rectangular cross section.

whole surface. The layer is pre-baked, flood exposed for 30 s and baked at 95 °C for 10 min. This layer was used as a transparent adhesion layer for the forthcoming thick SU-8 layer that showed poor adhesion on glass substrates.

**SU-8.** A thick layer of SU-8 2010 was poured on the surface of the sample without spin-coating. In fact, since the exposure was made through the backside, a regular and perfectly flat layer of photoresist is not needed. The process only required the SU-8 thickness to be higher than the thicker channel to be made (about 150 μm in our case). After 30 min of relaxation, the temperature of the thick SU-8 layer was ramped up (3 to 4 °C $min^{-1}$) to 95 °C and pre-baked for 30 min followed by a slow ramp down to room temperature. Due to thermal inertia of the hot plate, the ramp down to room temperature was more than one hour long. Other viscosities of SU-8 photoresist can be used as long as the final thickness of the layer is higher than that of the thicker channel to be processed.

**UV exposure.** Exposure was then made through an opal diffuser (75 mm opal diffuser #46-662, Edmund Optics, Barrington, NJ, USA) in direct contact with the backside of the glass. The sample is placed upside down on a dark plastic sheet to avoid optical reflections. The proper UV dose (mJ $cm^{-2}$) was optimized by a trial and error method starting from the energy recommended by the manufacturer. Several exposure times were thus tested ranging from 5 s to 30 s using a mercury vapor lamp and a long pass UV filter (PL-360LP, Omega Optical, Brattleboro, VT, USA) to eliminate UV radiation below 360 nm. We found that the suitable exposure time was around 16 s for our masker, and thus an equivalent dose of 160 mJ $cm^{-2}$ was used since our masker has an irradiance of 10 mW $cm^{-2}$, this dose being usually appropriate for a 50 μm thick SU-8 layer exposed trough conventional topside exposure.

**Development and hard bake.** Samples were then post-baked with a slow ramp up (3 to 4 °C $min^{-1}$) to 95 °C for 30 min and slowly ramped down to room temperature. Development was made in propylene glycol methyl ether acetate (PGMEA) until completion. This takes usually more than 30 min since the initial thickness of the resin was about several hundreds of microns. Finally, a hard-bake step was performed to soften the surfaces (ramp up to 160 °C for 30 minutes followed by a slow cooling to room temperature).

## Microfluidic replicas

PDMS microfluidic chips were fabricated using standard procedures. A 10 : 1 mix of PDMS and curing agents was prepared. The mixture was then poured on the samples, degassed for 30 min under vacuum and cured at 80 °C for two hours. Since SU-8 structures were rounded, showing negative clearance at some places, a silanization step was added to avoid attachment of PDMS on SU-8 and ease the unmoulding of the PDMS. It consisted in dipping the device for two hours in a hexane/(3-aminopropyl)triethoxysilane (APTES) solution followed by an ethanol rinsing, $N_2$ drying and hotplate baking at 120 °C for 20 min with slow temperature ramps. After dissection and extraction, the PDMS circuits were then punched to create the inlet and outlet and intensely washed with DI water and ethanol. Finally, the

 

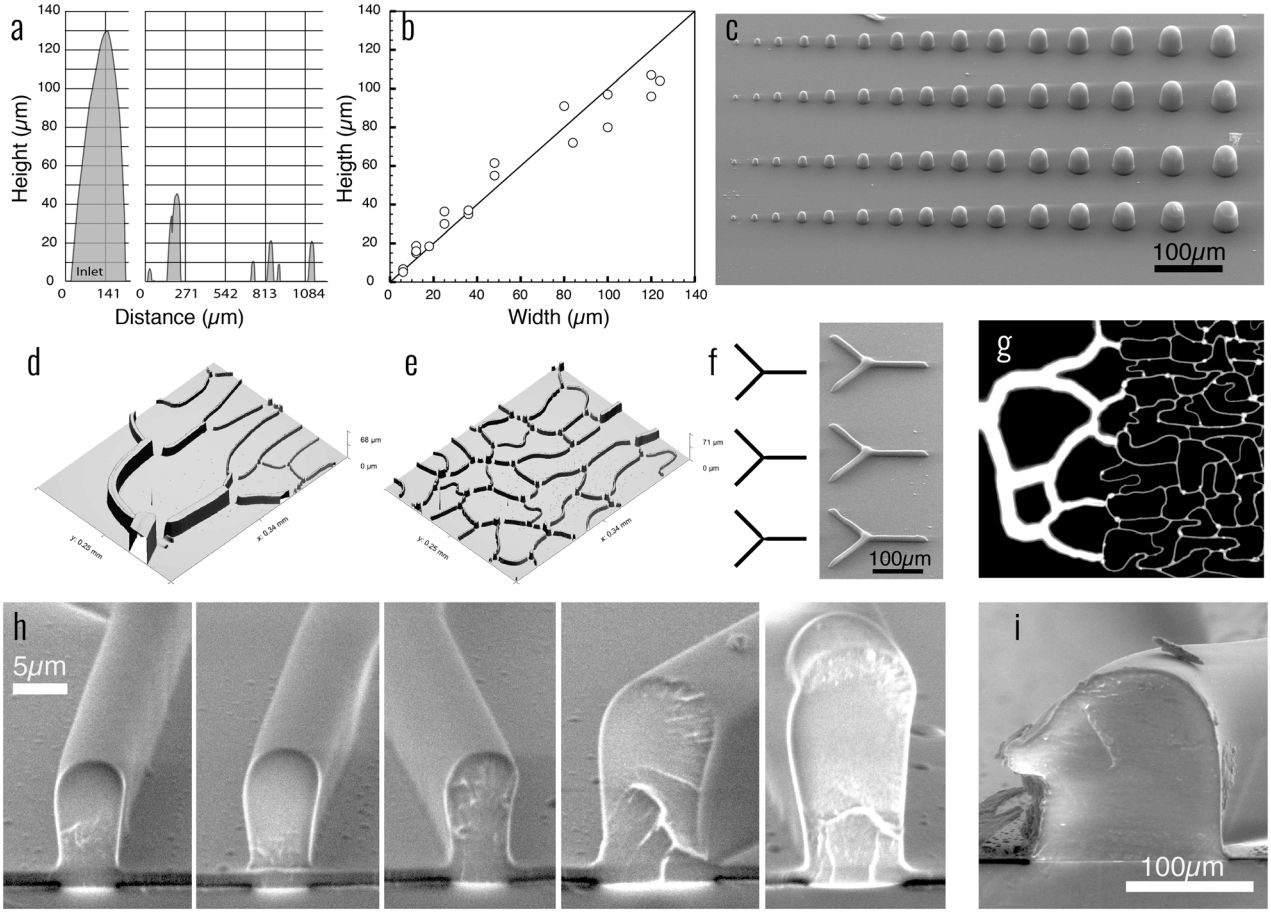


**Fig. 3** Topography analysis of the network. (a) Profiles of the SU8 patterns measured with a Dektak profilometer along arbitrary lines perpendicular to the inlet–outlet axis; the distribution of thicknesses ranges from 130 down to 5 μm. (b) Thickness of channels according to their nominal width on the photomask measured with the same technique. (c) SEM picture of test structures showing an array of domes obtained with circular openings ranging from 8 to 36 μm diameter. (d and e) Surface profile of different parts of the network made with optical interferometry. (f) Study of the effect of bifurcation shapes. Bifurcation with continuously thick lines on the mask (top) shows bumps at the node; the effect is reduced by thinning the lines at the nodes (middle and bottom). (g) Fluorescence measurement using rhodamine B as perfusing liquid; the intensity of fluorescence is proportional to the channel thickness. (h) SEM images of cleaved SU-8 channels showing the cross section of 5 and 8 μm capillaries and (i) the arteriole.

chips were treated with oxygen plasma (Plasmasystem Nano, Diener electronic GmbH, Ebhausen, Germany), allowing a permanent bonding on a standard 170 μm thick glass microscope slide.

**Circuit preparation.** Before blood flow experiments, PDMS circuits were hydrophylised using oxygen plasma in order to completely wet the capillary bed that can show high hydraulic resistance. Finally, 0.1% bovine serum albumin was perfused for 10 min in the chip in order to prevent blood clogging.

## Microscopy and characterization

**Optical microscopy.** Blood flow analysis was made using an inverted microscope (Zeiss Axiovert 200, Carl Zeiss GmbH, Oberkochen, Germany) with several objectives ranging from 4× to 100×. Images and movies were captured using a blue filter to enhance the contrast over RBCs and a camera fitted with a 2048 × 2048 pixel CMOS sensor (UI-3370CP, IDS Imaging Development Systems GmbH, Obersulm, Germany). Fast capture imaging was performed at frame rates of from 60 up to 1500 fps in order to observe individual cell movements.

**Profilometry.** Topology analyses were made using both mechanical and optical profilometers. Channel heights were measured using a Veeco Dektak 150 profiler (Veeco, Plainview, NY, USA) and images were taken using a Fogale Zoomsurf optical profilometer (Fogale Nanotech, Nîmes, France).

**SEM.** Samples were analysed using an FEI Inspect scanning electron microscope (ThermoFisher Scientific, Waltham, MA, USA) under environmental SEM conditions, *i.e.* at 0.8 mbar pressure and in the presence of vapour. Prior to this, the samples were metallized with 100 nm titanium using plasma sputtering.

**Hydrodynamic characterisation.** The velocity of RBCs was estimated using particle image velocity (ImageJ plugin) as illustrated in Fig. 5(c). The flow rate resulted from the product of the average velocity across the main arteriole (inlet vessel) and the cross-sectional area of the main arteriole. The overall

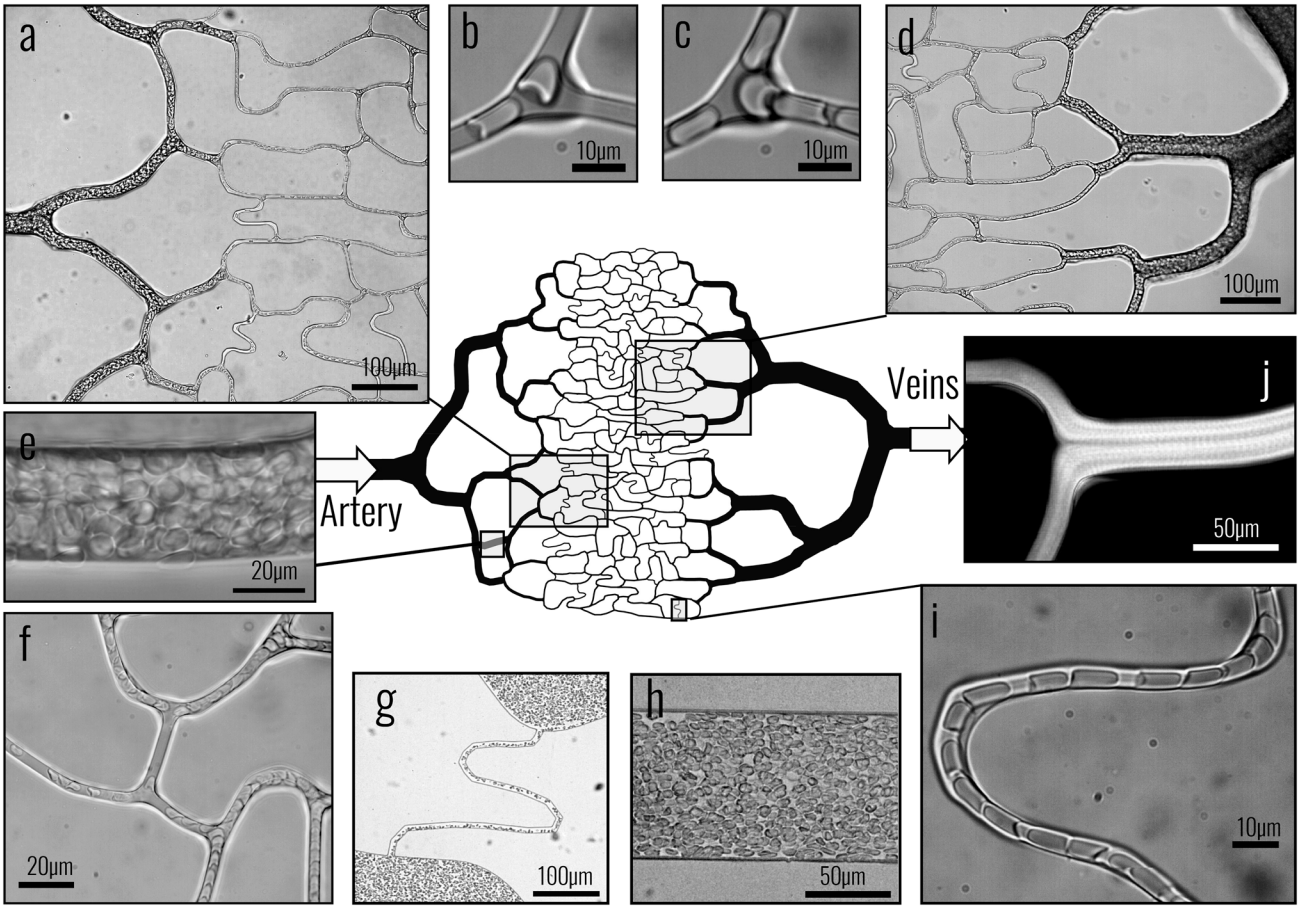


**Fig. 4** Videomicroscopy capture of blood flow experiments into artificial vascular networks. (Center) Layout of the global circuit showing the network between the inlet and the outlet. (a and d) Arterioles and veinules of the network. (b and c) Close up view of RBCs flowing in a bifurcation at high (200 mbar) and low (10 mbar) pressure, respectively. (e) Close up view of blood flow in arteriole showing the cell density and compaction. (f) Close up view of RBC flow in the capillary bed showing the difference of cell density in the capillaries. (g and h) Capture of blood flow in standard microfluidic circuit, *e.g.* with 15 μm constant thickness, within large and thin channels. We can notice that RBCs flow in the same plane, forming a single layer of cells. (i) Close up view of RBCs flowing in a capillary under high inlet pressure (200 mbar); we can observe the deformation of RBCs in a string of parachute-shaped cells. (j) Superposition of video sequence frames (standard deviation) showing the local density of cells in a veinule bifurcation.

network hydraulic resistance was then estimated as the ratio of the inlet pressure to the flow rate. In addition, the network flow distribution was investigated visually by manually counting the number of capillaries that were not flowing, named as "no flow". Finally, the local linear density of the RBCs in the capillaries was estimated and reported as the average of RBC count aligned in 100 μm.

### Blood samples

Venous blood samples were obtained from the local blood bank (Etablissement Francais du Sang, Montpellier, France). Whole blood was then centrifuged at 1000*g* for 20 min. Plasma and buffy coat, *i.e.* the fraction of the centrifuged blood sample containing most of the white blood cells and platelets, were removed. RBCs were then washed 3 times in PBS, followed by suspending the cells in the buffer solution and repeating the centrifugation and removal process. Afterward, the cells were resuspended in an Optiprep (Sigma Aldrich, Ref. D1556) based solution, composed of 67% PBS and 33% Optiprep and complemented with 0.9 mg $ml^{-1}$ glucose. Optiprep was used to match the typical mean density of RBC and avoid sedimentation in the tubing. The final hematocrit was adjusted to 45%. The entire process was done at room temperature. The blood suspension was then introduced into the microfluidic chip and flowed using a microfluidic pressure controller (Elveflow OB1, Elvesys SAS, Paris, France). Experiments were done under pressures ranging from 1 up to 800 mbar. A total of four 1 ml aliquots of blood suspension were used during the experiments on a dozen microfluidic chips.

## Results and discussion

### Microfluidic vascular replicas

**Topology.** The microfabricated network, as observed by SEM imaging (secondary electrons, Fig. 2(b–d)), shows that the channels exhibit a gradation of their thicknesses

 

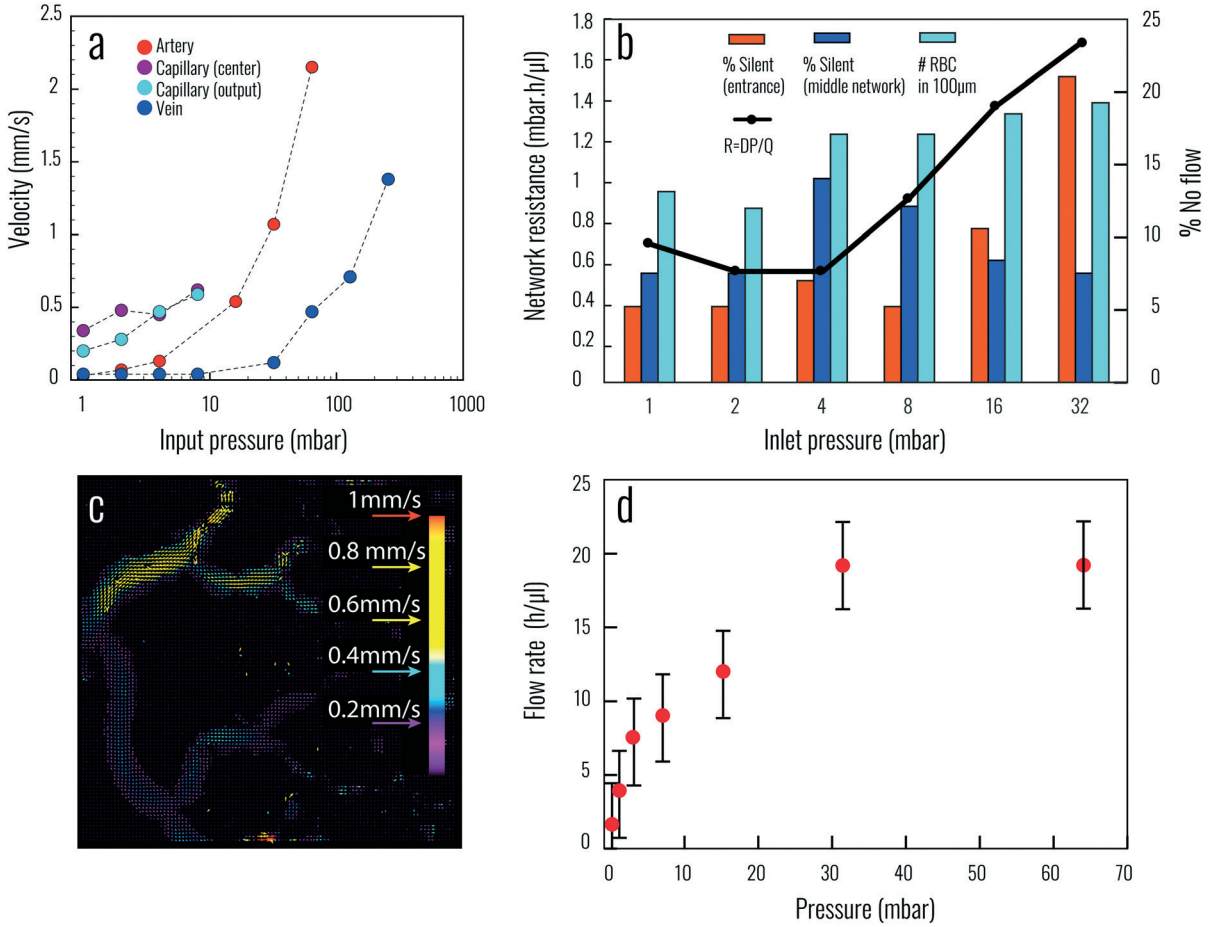


**Fig. 5** Flow and velocity analysis in the network. (a) Velocity of RBCs as a function of input pressure at the inlet at different locations of the network: artery, center capillary, output capillary and vein. (b) Hydraulic resistance of the network $R = DP/Q$ as a function of the inlet pressure. The red and blue bars indicate the percentage of capillaries that are not flowing ("% no flow") at the entrance and in the center of the network, respectively. The cyan bars present the linear red blood cell density in the capillary, *i.e.* the average RBC count per 100 μm. (c) Example of particle image velocimetry processing at the entrance of the network with an input pressure of 16 mbar. (d) Total flow rate as a function of the input pressure. Error bars present the uncertainty of the flow rate estimation due to an error of ±2 pixels per frame in the PIV measurement (which correspond to ±2.94 μl $h^{-1}$).

according to their widths. Thickness measurements obtained using a stylus profilometer are reported in Fig. 3(a). It shows that within the scanned line, channel thicknesses are about 130 μm for the inlet (120 μm initial width) and range from 50 μm down to 5 μm for arterioles and capillaries. However, this profilometry technique does not allow obtaining the exact profile of the section since the latter is convoluted by the conical shape and the velocity of the scanning probe. Fig. 3(b) shows the thickness of channels according to their nominal width on the photomask; despite some relative variations it shows a rather linear evolution from 5 up to 130 μm.

**Section.** Blood vessels *in vivo* show an almost circular cross section, so microfluidic replicas of vascular network should provide channels with a circular section. The backside illumination technique allows producing rounded sections, at least a section that is an image of the angular distribution of light intensity produced by the diffuser. In our case, we found that indeed the cross sections are rounded, as can be observed in Fig. 3(h and i). This has to be compared with the channels made with standard frontside lithography in Fig. 2(e and f). This can also be observed in the test structure in Fig. 3(c) that shows the results of circular openings in the mask ranging from 8 up to 36 μm diameter. By observing the cross sections of capillary channels we can also notice the presence of a clearance angle that makes the width of channels larger on their top part than at the base. In order to obtain more circular cross sections, such as the ones obtained by Lee *et al.*,[31] one possibility would be to increase the exposure time but this requires also lowering the width of openings in the mask.

**Roughness.** We also noticed that the surface of the SU-8 channels showed some irregularities and a certain roughness. This was due to inhomogeneities of the light scattered from the backside. This roughness can be softened by a hard bake of the SU-8 photoresist. Inlets and outlets were defined by 2 mm diameter circles and these wide openings created some rounded domes that receive the inlet and outlet tubing

through the PDMS slab. These large structures helped the introduction of blood samples in microchannels, avoiding clogging effects that often happen in conventional microfluidics.

**Bumps at nodes.** The backside illumination technology has some specificities regarding conventional lithography. Indeed, as we have shown before, the resulting height of microchannels was proportional to the width of the channels in the mask. When a bifurcation is drawn, the local surface is of a higher dimension than the main part of the channels. This creates some bumps, or domes, at the location of bifurcations, as can be observed in SEM pictures in Fig. 2(d) and in the fluorescence image in Fig. 3(g) where the intensity of fluorescence is proportional to the thickness. This effect can be reduced by locally thinning the line at bifurcations at the mask design level. This can be observed in Fig. 3(f) that shows three different designs of bifurcations with increasing level of local thinning (from top to bottom). The results shown in the SEM picture in Fig. 3(f) show a lowering of bifurcation bump height with local width thinning.

### Blood flow experiments

Microfluidic circuits made with the fabrication process that we presented here have been used to observe some particularities of blood flows. Fig. 4 shows some capture of 45% hematocrit blood flows in the network at different locations including arterioles, capillaries, bifurcations and veins.

### Comparisons with circuits of uniform height

When comparing the distribution of RBCs flowing in our vascular network with blood flowing into circuits with uniform height (Fig. 4(g and h)), the first observation that can be made is the difference in compaction of the cells. Indeed, as can be observed in Fig. 4(e), the arterioles are filled with high hematocrit blood and the cells are strongly compacted without spaces between them. This could be compared to Fig. 4(g and h) in which blood flows in a standard microfluidic circuit with a uniform thickness of 15 μm, forming a single layer of cells and a spatial distribution in a single plane.

Another observation that can be made using these vasculature replicas is the fact that they contain thick and thin channels that are not in the same focal plane. This differs from standard microfluidic circuits where every channel is on the same plane. This can be observed in Fig. 4(d) and Video S2 (ESI†) showing that large and thick channels appear blurry compared to the thin ones because they are located outside the focal plane. Light absorption by the RBCs is also worth noting. We can notice, in Fig. 4(a and d), that blood flowing into large and thick artery replicas absorbs a large part of the transmitted light, appearing darker than that in the capillaries and thus making it difficult to observe and to spatially resolve all RBC displacements, in contrast to those into slit-like channels (Fig. 4(g and h)).

### Local hematocrit

By observing the blood flow in channels with different sections, *e.g.* cells in the capillary bed *versus* the arteriole or veinule part of the network (Fig. 4(f) and Video S2 (ESI†), for example), we can observe that cells are traveling in the capillary bed with a lower hematocrit and that they have a different compaction compared with larger channels. This is called the network Fåhræus effect and it is caused by the fact that RBCs tend to move towards regions of low shear in the center of a vessel. This has been observed not only *in vivo*[38] but also in microfluidic vascular networks.[39] We can also notice that some capillaries are "silent" for some input pressure conditions, meaning that a low number of cells is actually flowing in them. Fig. 5(d) shows a measurement of the percentage of "silent" capillaries at the entrance and at the center of the capillary bed as a function of the input pressure. We can notice that these percentages were not constant and changed with the input pressure. The increase in inlet pressure leads to an increase in the flow rate and average velocity of the cells. This also leads to an increase in the shear rate, but also, consequently, to a change in cell shape and apparent blood viscosity. As a result, the distribution of pressure throughout the network is changed, which will induce local changes at the inlet and outlet of the capillary sections. For each input pressure value, a dynamic equilibrium will emerge and lead to different cell flows in each portion of the circuit and finally in some cases of silent sections.

**RBC shape and deformation.** The RBC shape is strongly modified when cells arrive in small capillaries, as shown in Fig. 4(b, c, f and i) and Video S1 (ESI†). Here RBCs adopt the typical parachute/bullet shape and their distribution is not homogeneous across the capillary. This effect is attributed to the hydrodynamic interaction between RBCs producing groups or trains of cells. This effect has been studied in detail *in vitro*,[34–36] but also parachutes and cluster formation have been observed in *in vivo* experiments.[37] Our artificial network allows mimicking in a more accurate way a physiological capillary bed, where curvatures and bifurcations are always present.

**Bifurcations.** Fig. 4(b and c) and Video S1 (ESI†) show the behaviour of RBCs crossing a bifurcation at high (200 mbar) and low (10 mbar) input pressure, respectively. We can first notice the change in shape of the cells that show a parachute shape for high input pressure and discocyte shape for lower pressure. Due to the presence of bumps at the nodes, the channel section at bifurcations increases and then we can observe some changes in the shape of the cells due to a relaxation of the cells when they pass through the bifurcation. This demonstrates the high deformability of the RBCs that adapt their shape to fit the dimensions of the vessel where they flow.

**Cell-free layer.** For certain blood flow conditions, a cell-free layer (CFL) may appear near the walls of the vessel in which the blood flows.[41] This region depleted in cells is due to competition between hydrodynamic interactions between

 

cells and the wall, which tends to repel cells, and by cell–cell hydrodynamic interactions, which on the contrary tend to disperse RBCs. The size of this CFL is known to be in the range of one to two microns for 45% Ht blood flowing in vessels from 10 to 50 μm;[42,43] this value increases as the hematocrit decreases. This value of the CFL being small has been difficult to observe in our experiments. However, we found that in the veinule part of the network, a CFL was present, especially after the junction of thinner channels as can be observed in Fig. 4(j). This effect is visible in the figure where we have superimposed about a hundred images taken in video by the standard deviation method on ImageJ. It can therefore be observed that the cells concentrate in the central part of the channel, forming a CFL near the walls and also in between both cell tubes; this distribution continues for a long distance after the bifurcation.

**Velocity *vs.* pressure.** The particle image velocimetry technique has been used to extract the RBC velocity in different parts of the network and for different input pressures. The results are shown in Fig. 5(a) where the cell velocities have been recorded in arteries, at two locations of the capillary bed (center and near the output) and in the vein part of the network. We can first notice that the velocity of the cells increases more with the input pressure in the arteries than in the veins. This is because, by design, the vein network is slightly larger on average than the artery network. As shown in Fig. 5(d), the flow rate does not increase linearly with an increase of pressure as is expected for Newtonian flow in a single channel. Therefore, the overall hydraulic resistance of the network is not constant, as shown in Fig. 5(b). Although these preliminary results do not allow concluding with certainty on the origin of this non-linearity, it could be explained by the inhomogeneity of the flow repartition and the inhomogeneity of the cell density in the network. Indeed, when some capillaries are not perfused, this results in a higher flow rate in the other capillaries and the total length of the capillaries perfused decreases. In addition, the linear density of cells increases with the increase of input pressure, as shown in Fig. 5(b). The increase of local cell density is likely linked with an increase of the local viscosity[40] and therefore an increase of the hydraulic resistance.

## Conclusions

This paper presented a novel microfabrication technique to produce artificial vascular networks whose geometry is close to that of natural vasculatures. The process is carried out by producing an SU-8 photoresist mould using a combination of backside illumination with an optical diffuser making it possible to obtain rounded cross section channels with a gradation of the thickness relative to their width with just one single mask. This new technology allows obtaining vascular networks that approach *in vivo* geometries for studying hemophysics and hemorheology. These circuits could also be used in the future as an imprint for epithelial cell culture in order to develop *in vitro* networks that could be the base of complex vascularised organs-on-chips.[43] This lithography technique can also be used in fields other than vascular networks, such as the shaping of branched hydrogel structures for mechanobiology or the capture of single cells. Finally, on the physical side, these devices will be used to investigate more in detail the relations between flow in the network and inlet pressure and especially the non-linearities of hydraulic resistance we observed.

## Author contributions

Conceptualization: B. C., V. G., M. F. and M. A. Methodology: B. C., M. F., V. C. and M. A. Microfabrication: B. C., V. G., and S. M. Experimental investigations: B. C., V. C., M. F. and S. M. Writing – review and editing: B. C., V. C., M. F. and M. A. Supervision: B. C.

## Conflicts of interest

There are no conflicts to declare.

## Acknowledgements

This work was supported by the LabEx NUMEV "Digital and Hardware Solutions, Environmental and Organic Life Modeling" (ANR-10-LABX-20-01) and by National Science and Engineering Research Council of Canada (#RGPIN-2015-06188).

## Notes and references

1 S. Chien, *et al.*, Blood viscosity: influence of erythrocyte aggregation, *Science*, 1967, **157**, 829–831.
2 L. Lanotte, *et al.*, Red cells' dynamic morphologies govern blood shear thinning under microcirculatory flow conditions, *Proc. Natl. Acad. Sci. U. S. A.*, 2016, 201608074.
3 A. R. Pries, T. W. Secomb, P. Gaehtgens and J. F. Gross, Blood flow in microvascular networks. Experiments and simulation, *Circ. Res.*, 1990, **67**, 826–834.
4 K. H. K. Wong, J. M. Chan, R. D. Kamm and J. Tien, Microfluidic Models of Vascular Functions, *Annu. Rev. Biomed. Eng.*, 2012, **14**, 205–230.
5 B. Sebastian and P. S. Dittrich, Microfluidics to Mimic Blood Flow in Health and Disease, *Annu. Rev. Fluid Mech.*, 2018, **50**, 483–504.
6 S. S. Shevkoplyas, S. C. Gifford, T. Yoshida and M. W. Bitensky, Prototype of an in vitro model of the microcirculation, *Microvasc. Res.*, 2003, **65**, 132–136.
7 R. Lima, *et al.*, In vitro blood flow in a rectangular PDMS microchannel: experimental observations using a confocal micro-PIV system, *Biomed. Microdevices*, 2008, **10**, 153–167.
8 S. Roman, A. Merlo, P. Duru, F. Risso and S. Lorthois, Going beyond 20 μm-sized channels for studying red blood cell phase separation in microfluidic bifurcations, *Biomicrofluidics*, 2016, **10**, 034103.
9 R. Mehri, J. Laplante, C. Mavriplis and M. Fenech, Investigation of Blood Flow Analysis and Red Blood Cell Aggregation, *J. Med. Biol. Eng.*, 2013, **34**, 469–474.

10 O. Forouzan, X. Yang, J. M. Sosa, J. M. Burns and S. S. Shevkoplyas, Spontaneous oscillations of capillary blood flow in artificial microvascular networks, *Microvasc. Res.*, 2012, **84**, 123–132.
11 M. Fenech, D. Garcia, H. J. Meiselman and G. Cloutier, A Particle Dynamic Model of Red Blood Cell Aggregation Kinetics, *Ann. Biomed. Eng.*, 2009, **37**, 2299–2309.
12 D. M. Lewis, H. E. Abaci, Y. Xu and S. Gerecht, Endothelial progenitor cell recruitment in a microfluidic vascular model, *Biofabrication*, 2015, **7**, 045010.
13 M. Raasch, *et al.*, Microfluidically supported biochip design for culture of endothelial cell layers with improved perfusion conditions, *Biofabrication*, 2015, **7**, 015013.
14 R. Thuenauer, E. Rodriguez-Boulan and W. Römer, Microfluidic approaches for epithelial cell layer culture and characterisation, *Analyst*, 2014, **139**, 3206–3218.
15 L. Lanotte, G. Tomaiuolo, C. Misbah, L. Bureau and S. Guido, Red blood cell dynamics in polymer brush-coated microcapillaries: A model of endothelial glycocalyx in vitro, *Biomicrofluidics*, 2014, **8**, 014104.
16 J. M. Burns, X. Yang, O. Forouzan, J. M. Sosa and S. S. Shevkoplyas, Artificial microvascular network: a new tool for measuring rheologic properties of stored red blood cells, *Transfusion*, 2012, **52**, 1010–1023.
17 S. S. Shevkoplyas, T. Yoshida, S. C. Gifford and M. W. Bitensky, Direct measurement of the impact of impaired erythrocyte deformability on microvascular network perfusion in a microfluidic device, *Lab Chip*, 2006, **6**, 914–920.
18 Q. Wu, *et al.*, Microfabrication of polydimethylsiloxane phantoms to simulate tumor hypoxia and vascular anomaly, *J. Biomed. Opt.*, 2015, **20**, 121308.
19 I. D. Kelch, *et al.*, Organ-wide 3D-imaging and topological analysis of the continuous microvascular network in a murine lymph node, *Sci. Rep.*, 2015, **5**, 16534.
20 G. R. Cokelet, R. Soave, G. Pugh and L. Rathbun, Fabrication of in vitro microvascular blood flow systems by photolithography, *Microvasc. Res.*, 1993, **46**, 394–400.
21 X. Yang, O. Forouzan, J. M. Burns and S. S. Shevkoplyas, Traffic of leukocytes in microfluidic channels with rectangular and rounded cross-sections, *Lab Chip*, 2011, **11**, 3231–3240.
22 L. K. Fiddes, *et al.*, A circular cross-section PDMS microfluidics system for replication of cardiovascular flow conditions, *Biomaterials*, 2010, **31**, 3459–3464.
23 D. Lim, Y. Kamotani, B. Cho, J. Mazumder and S. Takayama, Fabrication of microfluidic mixers and artificial vasculatures using a high-brightness diode-pumped Nd:YAG laser direct write method, *Lab Chip*, 2003, **3**, 318–323.
24 X. Li, L. Liu, X. Zhang and T. Xu, Research and development of 3D printed vasculature constructs, *Biofabrication*, 2018, **10**, 032002.
25 D. B. Kolesky, R. L. Truby, A. S. Gladman, T. A. Busbee, K. A. Homan and J. A. Lewis, 3D bioprinting of vascularized, heterogeneous cell-laden tissue constructs, *Adv. Mater.*, 2014, **26**, 3124–3130.
26 D. P. Parekh, C. Ladd, L. Panich, K. Moussa and M. D. Dickey, 3D printing of liquid metals as fugitive inks for fabrication of 3D microfluidic channels, *Lab Chip*, 2016, **16**, 1812–1820.
27 H. H. Lipowsky and B. W. Zweifach, Network analysis of microcirculation of cat mesentery, *Microvasc. Res.*, 1974, **7**, 73–83.
28 R. W. Barber and D. R. Emerson, Optimal design of microfluidic networks using biologically inspired principles, *Microfluid. Nanofluid.*, 2008, **1**, 179–191.
29 Y.-C. Chen, G.-Y. Chen, Y.-C. Lin and G.-J. Wang, A lab-on-a-chip capillary network for red blood cell hydrodynamics, *Microfluid. Nanofluid.*, 2010, **9**, 585–591.
30 N. Futai, W. Gu and S. Takayama, Rapid Prototyping of Microstructures with Bell-Shaped Cross-Sections and Its Application to Deformation-Based Microfluidic Valves, *Adv. Mater.*, 2004, **16**, 1320–1323.
31 J.-H. Lee, W.-S. Choi, K.-H. Lee and J.-B. Yoon, A simple and effective fabrication method for various 3D microstructures: backside 3D diffuser lithography, *J. Micromech. Microeng.*, 2008, **18**, 125015.
32 D. Lai, *et al.*, Simple multi-level microchannel fabrication by pseudo-grayscale backside diffused light lithography, *RSC Adv.*, 2013, **3**, 19467–19473.
33 M. Kang, J. H. Byun, S. Na and N. L. Jeon, Fabrication of functional 3D multi-level microstructures on transparent substrates by one step back-side UV photolithography, *RSC Adv.*, 2017, **7**, 13353–13361.
34 V. Claveria, *et al.*, Cluster of red blood cells in microcapillary flow: hydrodynamic versus macromolecule induced interaction, *Soft Matter*, 2016, **12**, 8235–8245.
35 G. Tomaiuolo, L. Lanotte, G. Ghigliotti, C. Misbah and S. Guido, Red bloodcell clustering in poiseuille microcapillary flow, *Phys. Fluids*, 2012, **24**(5), 051903.
36 J. L. McWhirter, H. Noguchi and G. Gompper, Deformation and clustering of red blood cells in microcapillary flows, *Soft Matter*, 2011, **7**(22), 10967–10977.
37 R. Skalak and P. Branemark, Deformation of red blood cells in capillaries, *Science*, 1969, **9**(164), 717–719.
38 H. H. Lipowsky, S. Kovalcheck and B. W. Zweifach, The distribution of blood rheological parameters in the microvasculature of cat mesentery, *Circ. Res.*, 1978, **43**, 738–749.
39 W. H. Reinhart, N. Z. Piety and S. S. Shevkoplyas, Influence of feeding hematocrit and perfusion pressure on hematocrit reduction (Fåhraeus effect) in an artificial microvascular network, *Microcirculation*, 2017, **24**(8), e12396.
40 N. Z. Piety, W. H. Reinhart, J. Stutz and S. S. Shevkoplyas, Optimal hematocrit in an artificial microvascular network, *Transfusion*, 2017, **57**(9), 2257–2266.
41 S. Kim, P. K. Ong, O. Yalcin, M. Intaglietta and P. C. Johnson, The cell-free layer in microvascular blood flow, *Biorheology*, 2009, **46**(3), 181–189.
42 D. A. Fedosov, B. Caswell, A. S. Popel and G. E. M. Karniadakis, Blood Flow and Cell-Free Layer in Microvessels, *Microcirculation*, 2010, **17**(8), 615–628.

 

43 D. Bento, A. I. Pereira, J. Lima, J. M. Miranda and R. Lima, Cell-free layer measurements of in vitro blood flow in a microfluidic network: an automatic and manual approach, *Comput. Methods Biomech. Biomed. Eng. Imaging Vis.*, 2018, **6**, 629–637; D. Tsvirkun, A. Grichine, A. Duperray, C. Misbah and L. Bureau, Microvasculature on a chip: study of the Endothelial Surface Layer and the flow structure of Red Blood Cells, *Sci. Rep.*, 2017, **7**, 45036.